ISSN: 0975-833X

Available online at http://www.journalcra.com

International Journal of Current Research
Vol. 13, Issue, 02, pp.16084-16101, February, 2021

DOI: https://doi.org/10.24941/ijcr.40704.02.2021

INTERNATIONAL JOURNAL OF CURRENT RESEARCH

RESEARCH ARTICLE

EVAPORATION IMPROVEMENT IN NATURAL CONVECTION OF HEPTANE LIQUID DROPLET

DABILGOU Téré[1,3,*], DGHEIM Joseph [2], SANDWIDI Sayouba[1,3], DAHO Tizane[1], ZONGO S. Augustin [1], CHESNEAU Xavier[3] , , KOULIDIATI Jean[1], SANOGO Oumar[4], ZEGHMATI Belkacem[3] and BERE Antoine[1]

[1]Laboratoire de Physique et de Chimie de l'Environnement (LPCE), Université Joseph KI-ZERBO, 03 BP : 7021 Ouagadougou 03, Burkina Faso
[2]Laboratoire de Physique Appliqué, Groupe de Mécanique Thermique et Énergies Renouvelables LPA-GMTER, Université Libanaise
[3]Laboratoire de Mathématiques et Physiques (LAMPS), Université de Perpignan Via Domitia : 52, avenue Paul Alduy-66100 Perpignan, France
[4]Centre National de la Recherche Scientifique et Technologique (CNRST) /Institut de Recherche en Sciences Appliquées et Technologies (IRSAT), 03 BP 7047 Ouagadougou 03, Burkina Faso

ARTICLE INFO

Article History:
Received 27th November, 2020
Received in revised form
29th December, 2020
Accepted 20th January, 2021
Published online 26th February, 2021

Key Words:
Droplet evaporation,
Heat & Mass Transfer,
Evaporation,
Conservation equation,
Heptane Droplet.

ABSTRACT

A numerical study of the evaporation by laminar natural convection of a heptane liquid droplet is presented. The classical boundary layer equations are used in the liquid phase and in the vapor phase. The transfers are described by the natural convection equations. The linkage between heat and mass transfer in the liquid and vapor phases is ensured by the continuity at the liquid vapor interface by the heat and mass flux densities and the shear stresses. Dimensionless equations in the liquid and vapor phases are solved using an implicit numerical scheme and Thomas algorithm. One analyzes the effects of the gaseous medium temperature and the initial droplet radius values on the profiles of the temperature and radial velocity in both phases, of the heptane vapor fraction in the gaseous medium and of the vapor phase thickness. Thus, the vapor phase thickness is calculated and presented versus time for different physical parameters especially the theta angle. The none-sphericity of the evaporated heptane droplet is clearly observed.

Citation: ***DABILGOU Téré, DGHEIM Joseph, SANDWIDI Sayouba, DAHO Tizane et al., 2021*** "Evaporation improvement in natural convection of heptane liquid droplet", *International Journal of Current Research*, 13, (02), 16084-16101.

INTRODUCTION

The phenomena of evaporation of fuel droplets have been the subject of considerable attention by many researchers (Chesneau 1994; Godsave 1953; Abramzon & Sirignano 1989; Dgheim *et al*. 2013; Sazhin 2018) since several years due to their direct relevance in many engineering applications such as internal combustion engine, burners, turbo-machines, etc... The recent development of the numerical techniques has contributed to the rise of numerical studies in the field of droplet evaporation such as those of liquid hydrocarbon. However, this field is very complex in particular when the phenomenon of two-phase flow occurs. It remains a largely important field for research. Despite the development of new numerical techniques which have made it possible to improve and take into consideration several physical parameters in evaporation phenomena, numerous studies (Tonini & Cossali 2012; Merouane 2013; Sazhin 2017; Dgheim *et al*. 2018) have not elucidated deeply the problems and difficulties still exist in the resolution of two-phase evaporation phenomena. However, studies undertaken by many researchers to solve these difficulties have made it possible to develop several numerical models and techniques (Zubkov *et al*. 2017; Qubeissi *et al*. 2015; Dgheim *et al*. 2017). Most of these models are oriented towards the temporal evolutions of the radius square and the surface temperature. Thus, the isolated droplet remains one of the studies of many researchers in the case of hydrocarbon droplet evaporation.

Corresponding author:** ***DABILGOU Téré,
[1]Laboratoire de Physique et de Chimie de l'Environnement (LPCE), Université Joseph KI-ZERBO, 03 BP : 7021 Ouagadougou 03, Burkina Faso
[3]Laboratoire de Mathématiques et Physiques (LAMPS), Université de Perpignan Via Domitia : 52, avenue Paul Alduy-66100 Perpignan, France.

From recent numerical and experimental studies on fuel droplet evaporation (Sazhin 2017; Pan et Chiu 2013; Ahmed *et al*. 2018; Nath, Pati & Raju 2018), it has been shown that many researchers are interested in this field in order to reasonably describe the essential phenomena which generate the processes involved in fuel evaporation & combustion. Indeed, in the case of isolated droplets, evaporation is governed mainly by the processes of heat and mass transfer. The knowledge gained from these processes is very important in the application of various spray patterns and combustion chamber geometries. Advances in the development of powerful and comprehensive numerical codes have a contributing part, although data obtained from single droplet studies play an important role in the success of the numerical models. In fact, the vaporization of fuels in engines has a strong influence on pollutant emissions, ignition delays and overall combustion efficiency (Khiari 2016; Daho 2008). When a droplet enters a warmer environment such as a combustion chamber, it is heated, evaporated and then burned to provide energy. Therefore, it is often difficult to isolate and study individual physical processes, mainly in environments where there are complicating factors such as the influence of thermophysical and physicochemical properties, ambient temperature, advection, etc... It is therefore useful to study the simplest configurations of the evaporation phenomenon. Vaporization of a single droplet has been widely studied in recent decades, both experimentally and numerically (Sardar *et al*. 2020; Pinheiro *et al*. 2019; Lupo & Duwig 2018; Frackowiak 2007; Dgheim *et al*. 2018). Most experimental studies on the evaporation of a droplet of liquid fuels, and more particularly heptane, are often very expensive and very complex. Hence it is increasingly resorting to numerical simulations. However, given the complexity of this topic, an isolated droplet evaporating in a gaseous medium which represents an ideal model of the physical phenomena involved in the dilute regions of a spray, seems to be a first step towards a better understanding of the dynamics of evaporation phenomenon. Studies focused on the evaporation of fuel droplets, in particular the heptane, in natural convection has not been the subject of intensive scientific study. Ahmed *et al*. 2018, Sazhin 2018, and Dgheim *et al*. 2020, studied the influence of the ambient temperature and the initial radius of the droplets on the burning rate. However, the influence of the thermophysical properties, the mass production rate and the advection especially in the liquid phase of the evaporated droplet where the theta angle is considered in the conservation equations, has not been fully investigated. In order to complete the previous studies, actual work aims to improve the heat and mass transfers of an isolated liquid fuel droplet, in natural convection evaporation**,** subjected to the influence of thermophysical properties by taking into account the effect of the mass production rate, the advection, and the influence of the theta angle in the transfers' equations, on fuel droplet physical parameters.

Physical model: The physical model consist of a fuel droplet of radius r_s immersed in an gaseous media. The pressure of this media is equal to one atmosphere and the temperature maintained at a temperature slightly higher than that of the liquid phase. This temperature difference generates a supply of heat by convection-conduction from the gas phase to the liquid one. Consequently the liquid temperature increases until to reach, if the amount of heat is sufficient, its temperature evaporation. Let us associate to this droplet a spherical reference frame such that the origin O coincides with the center of the droplet. The axis [oz) is vertical and oriented in the opposite direction to the gravity field vector. The [Ox) axis is perpendicular to [Oz) and oriented from left to right, and the [Oy) axis is perpendicular to the [O, y, [Oz)] plane as shown in Figure 1.

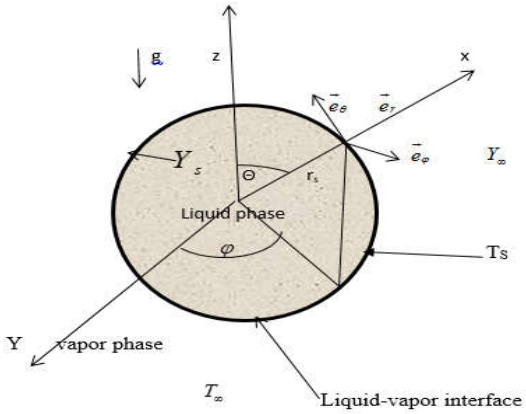

Figure 1. Diagram of the physical model

The physical phenomenon of the droplet evaporation are represented in Figure 2.

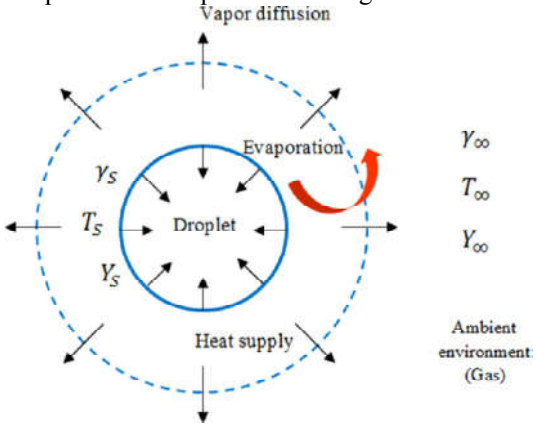

Figure 2. Physical phenomenon of a droplet evaporation in a stagnant medium

The literature reports that the evaporation of a mono-component droplet, in a stagnant medium, is the simplest model (Chahine & Dgheim 2017; Ahmed *et al*. 2018). In this case, the droplet is kept in the same environment as before, i.e. the temperature at the liquid surface (T_S) must initially be lower than the temperature of the surrounding medium, and the pressure of the medium is equal to the ambient pressure (1atm). Under these conditions, two phenomena occur (Mauduit 1992; Merouane 2013; Nje 2000):

- Heat transfer by conduction from the surrounding medium to the surface of the droplet increases the droplet temperature and evaporates partially this latter,
- Diffusion of the mass produced by the gaseous concentration gradient between the surface of the droplet and its surrounding environment allows the droplet to vaporize continually.

Simplifying Assumptions

- The gaseous media in which the hydrocarbon liquid droplet is placed is undisturbed.
- The transfers in the gaseous phase are laminar and are of the boundary layer type,
- The transfers admit symmetry azimutale
- The different gases and their mixtures behave like perfect gases,
- The Boussinesq approximation is retained in the equation of motion. The relative change in density obeys Boussinesq approximation,
- The effects of Soret and Dufour are negligible,
- The liquid-gaseous interface is in thermodynamic equilibrium,
- The kinetic chemical is infinitely fast,
- The surface tension is negligible,

Mathematical model: Taking account of the above assumptions, the equations governing the transfer in the liquid and gaseous phases can be written in the spherical reference (O,r,θ) as following:

Gaseous phase

Continuity equation

$$\frac{\rho_g}{r^2}\frac{\partial}{\partial r}\left(r^2 u_{rg}\right) + \frac{\rho_g}{r sin\theta}\frac{\partial}{\partial \theta}\left(u_{\theta g} sin\theta\right) = 0 \quad (1)$$

Momentum equation

$$\frac{\partial u_{rg}}{\partial t} + u_{rg}\frac{\partial u_{rg}}{\partial r} + \frac{u_{\theta g}}{r} = \frac{\mu_g}{\rho_g r^2}\frac{\partial}{\partial r}\left(r^2\frac{\partial u_{rg}}{\partial r}\right) + \quad (2)$$

$$\frac{\mu_g}{\rho_g}\frac{1}{r^2 sin\theta}\frac{\partial}{\partial \theta}\left(sin\theta\frac{\partial u_{rg}}{\partial \theta}\right) - g\beta_T\left(T_g - T_\infty\right)sin\theta - g\beta_M\left(Y_g - Y_\infty\right)sin\theta$$

Energy conservation equation

$$\frac{\partial T_g}{\partial t} + u_{rg}\frac{\partial T_g}{\partial r} + \frac{u_{\theta g}}{r}\frac{\partial T_g}{\partial \theta} = \frac{\lambda_g}{\rho_g Cp_g r^2}\frac{\partial}{\partial r}\left(r^2\frac{\partial T_g}{\partial r}\right) + \quad (3)$$

$$\frac{\lambda_g}{\rho_g Cp_g}\frac{1}{r^2 sin\theta}\frac{\partial}{\partial \theta}\left(sin\theta\frac{\partial T_g}{\partial \theta}\right) + \frac{1}{\rho_g Cp_g}\dot{\omega_g} Q_R \quad (4)$$

Diffusion equation

$$\frac{\partial Y_g}{\partial t} + u_{rg}\frac{\partial Y_g}{\partial r} + \frac{u_{\theta g}}{r}\frac{\partial Y_g}{\partial \theta} = \frac{\rho_g D_M}{\rho_g r^2}\frac{\partial}{\partial r}\left(r^2\frac{\partial Y_g}{\partial r}\right) \quad (5)$$

$$+\frac{\rho_g D_M}{\rho_g}\frac{1}{r^2 sin\theta}\frac{\partial}{\partial \theta}\left(sin\theta\frac{\partial Y_g}{\partial \theta}\right) + \frac{\dot{\omega_g}}{\rho_g}$$

where $\dot{\omega}_g$ is the mass production

$$\dot{\omega_g} = -\frac{3\rho D_M \frac{1}{r}\frac{\partial Y}{\partial \theta}}{(1 - Y_s)4\pi r_s^3}$$

Liquid phase

Continuity equation

$$\frac{\rho_l}{r^2}\frac{\partial}{\partial r}(r^2 u_{rl}) + \frac{\rho_l}{r sin\theta}\frac{\partial}{\partial \theta}(u_{\theta l} sin\theta) = 0 \quad (6)$$

Momentum equation

$$\frac{\partial u_{rl}}{\partial t} + u_{rl}\frac{\partial u_{rl}}{\partial r} + \frac{u_{\theta l}}{r}\frac{\partial u_{rl}}{\partial \theta} = \frac{\mu_l}{\rho_l r^2}\frac{\partial}{\partial r}\left(r^2\frac{\partial u_{rl}}{\partial r}\right)$$

$$+\frac{\mu_l}{\rho_l}\frac{1}{r^2\sin\theta}\frac{\partial}{\partial\theta}\left(\sin\theta\frac{\partial u_{rl}}{\partial\theta}\right) - g\beta_T(T_l - T_\infty)\sin\theta \quad (7)$$

Energy conservation equation

$$\frac{\partial \mathrm{T_l}}{\partial \mathrm{t}} + \mathrm{u_{rl}}\frac{\partial \mathrm{T_l}}{\partial \mathrm{r}} + \frac{\mathrm{u_{\theta l}}}{\mathrm{r}}\frac{\partial \mathrm{T_l}}{\partial \theta} = \frac{\lambda_\mathrm{l}}{\rho_\mathrm{l}\mathrm{Cp_l}\mathrm{r}^2}\frac{\partial}{\partial \mathrm{r}}\left(\mathrm{r}^2\frac{\partial \mathrm{T_l}}{\partial \mathrm{r}}\right)$$

$$+\frac{\lambda_\mathrm{l}}{\rho_\mathrm{l}\mathrm{Cp_l}}\frac{1}{\mathrm{r}^2\sin\theta}\frac{\partial}{\partial\theta}\left(\sin\theta\frac{\partial \mathrm{T_l}}{\partial\theta}\right) \quad (8)$$

Initial and boundary conditions

Initial conditions: $\forall\, t < t_0$,t_0 is the instant fromwhich the droplet is subjected to an input heat by convection-conduction. The temperature and the mass fraction are set equal to the surface temperature and surface mass fraction of the droplets.

$$T_l = T_0; \quad u_{rg0} = 0; \qquad u_{\theta g0} = 0 \quad (9)$$

$$Y_g = Y_{s0}; \qquad \mathrm{T}_g = \mathrm{T}_{s0} \quad (10)$$

IV.3.2. Boundary conditions:$\forall\, t > t_0$

-Center of the droplet: $r = 0$

-

$$\frac{\partial T}{\partial r} = 0; \qquad \frac{\partial u_{rl}}{\partial r} = 0; \qquad \frac{\partial u_{\theta l}}{\partial r} = 0 \quad (11)$$

Liquid-gaseous interface:$r = r_S$

$$-\lambda_g\frac{\partial T_g}{\partial r})_g = \lambda_l\frac{\partial T_l}{\partial r})_l + \rho_g D_M L\frac{\partial Y_g}{\partial r})_g \quad (12)$$

$$\mu_g\frac{\partial u_{\theta g}}{\partial r})_g = \mu_l\frac{\partial u_{\theta l}}{\partial r})_l \quad (13)$$

$$u_{\theta g} = -D_M\frac{\partial Y_g}{\partial r})_g \quad (14)$$

-Far from the droplet: $r \to \infty$

-

$$T_g = T_\infty; \qquad u_{rg} = u_{\theta g} = 0; \qquad \mathrm{Y}_g = 0 \quad (15)$$

Transformation of the coordinates: In order to avoid the non uniformity of the mesh in the vicinity of the liquid-vapor interface, the following transformation are used :

$$(t, r, \theta) \to (t, \eta = \frac{r}{r_s}, \theta) \quad (16)$$

$$\left.\frac{\partial}{\partial t}\right|_{t,r} = \frac{\partial}{\partial t}; \qquad \left.\frac{\partial}{\partial r}\right|_{t,r} = \frac{1}{r_s}\frac{\partial}{\partial \eta}$$
$$\left.\frac{\partial^2}{\partial r^2}\right|_{t,r} = \frac{1}{r_s^2}\frac{\partial^2}{\partial \eta^2}; \quad \left.\frac{\partial}{\partial\theta}\right|_{t,r} = \frac{\partial}{\partial\theta}; \quad \left.\frac{\partial^2}{\partial\theta^2}\right|_{t,r} = \frac{\partial^2}{\partial\theta^2} \quad (17)$$

In the new coordinate system the equations (1-8) are :
-Gaseous phase

$$\frac{\partial u_{rg}}{\partial \eta}+\frac{1}{\eta}\frac{\partial u_{\theta g}}{\partial \theta}+\frac{2u_{rg}}{\eta}+\frac{u_{\theta g}\cos(\theta)}{\eta\sin(\theta)}=0 \tag{18}$$

$$\frac{\partial u_{rg}}{\partial t}=\left(\frac{2\mu_g}{\rho_g r_s^2\eta}-\frac{u_{rg}}{r_s}\right)\frac{\partial u_{rg}}{\partial \eta}+\frac{\mu_g}{\rho_g r_s^2}\frac{\partial^2 u_g}{\partial \eta^2}+\left[\frac{\mu_g}{\rho_g r_s^2\eta^2}\frac{\cos(\theta)}{\sin(\theta)}-\frac{u_{\theta g}}{r_s\eta}\right]\frac{\partial u_{rg}}{\partial \theta}$$

$$+\frac{\mu_g}{\rho_g r_s^2\eta^2}\frac{\partial^2 u_{rg}}{\partial \theta^2}-g\beta_T\left(T_g-T_\infty\right)sin(\theta)-g\beta_M\left(Y_g-Y_\infty\right)sin(\theta) \tag{19}$$

$$\frac{\partial T_g}{\partial t}=\left(\frac{2\lambda_g}{\rho_g Cp_g r_s^2\eta}-\frac{u_{rg}}{r_s}\right)\frac{\partial T_g}{\partial \eta}+\frac{\lambda_g}{\rho_g Cp_g r_s^2}\frac{\partial^2 T_g}{\partial \eta^2}+\left[\frac{\lambda_g}{\rho_g Cp_g r_s^2\eta^2}\frac{\cos(\theta)}{\sin(\theta)}-\frac{u_{\theta g}}{r_s\eta}\right]\frac{\partial T_g}{\partial \theta}$$

$$+\frac{\lambda_g}{\rho_g Cp_g r_s^2\eta^2}\frac{\partial^2 T_g}{\partial \theta^2}+\frac{\dot{\omega}_g Q_R}{\rho_g Cp_g} \tag{20}$$

$$\frac{\partial Y_g}{\partial t}=\left(\frac{2D_M}{r_s^2\eta}-\frac{u_{rg}}{r_s}\right)\frac{\partial Y_g}{\partial \eta}+\frac{D_M}{r_s^2}\frac{\partial^2 Y_g}{\partial \eta^2}+\left[\frac{D_M}{r_s^2\eta^2}\frac{\cos(\theta)}{\sin(\theta)}-\frac{u_{\theta g}}{r_s\eta}\right]\frac{\partial Y_g}{\partial \theta}+\frac{D_M}{r_s^2\eta^2}\frac{\partial^2 Y_g}{\partial \theta^2}+\frac{\dot{\omega}_g}{\rho_g} \tag{21}$$

Liquid phase

$$\frac{\partial u_{rl}}{\partial \eta}+\frac{1}{\eta}\frac{\partial u_{\theta l}}{\partial \theta}+\frac{2u_{rl}}{\eta}+\frac{u_{\theta l}\cos(\theta)}{\eta\sin(\theta)}=0 \tag{22}$$

$$\frac{\partial u_{rl}}{\partial t}=\left(\frac{2\mu_l}{\rho_l r_s^2\eta}-\frac{u_{rl}}{r_s}\right)\frac{\partial u_{rl}}{\partial \eta}+\frac{\mu_l}{\rho_l r_s^2}\frac{\partial^2 u_l}{\partial \eta^2}+\left[\frac{\mu_l}{\rho_l r_s^2\eta^2}\frac{\cos(\theta)}{\sin(\theta)}-\frac{u_{\theta l}}{r_s\eta}\right]\frac{\partial u_{rg}}{\partial \theta}$$
$$+\frac{\mu_l}{\rho_l r_s^2\eta^2}\frac{\partial^2 u_{rl}}{\partial \theta^2}-g\beta_T(T_l-T_\infty)sin(\theta) \tag{23}$$

$$\frac{\partial T_l}{\partial t}=\left(\frac{2\lambda_l}{\rho_l Cp_l r_s^2\eta}-\frac{u_{rl}}{r_s}\right)\frac{\partial T_l}{\partial \eta}+\frac{\lambda_l}{\rho_l Cp_l r_s^2}\frac{\partial^2 T_l}{\partial \eta^2}+\left[\frac{\lambda_l}{\rho_l Cp_l r_s^2\eta^2}\frac{\cos(\theta)}{\sin(\theta)}-\frac{u_{\theta l}}{r_s\eta}\right]\frac{\partial T_l}{\partial \theta}$$
$$+\frac{\lambda_l}{\rho_l Cp_l r_s^2\eta^2}\frac{\partial^2 T_l}{\partial \theta^2} \tag{24}$$

The boundary conditions (11-15) are:

$$\eta=0:\left.\frac{\partial T_{lj}}{\partial \eta}\right|_{c,e}=0 \tag{25}$$

$$\eta=1:\mu_g\left.\frac{\partial u_{rg}}{\partial \eta}\right|_{sg}=\mu_l\left.\frac{\partial u_{rl}}{\partial \eta}\right|_{sl} \tag{26}$$

$$\lambda_g\frac{\partial T_g}{\partial \eta}=-\lambda_l\frac{\partial T_l}{\partial \eta}-\rho_g D_M Lv\frac{\partial Y_g}{\partial \eta} \tag{27}$$

$$u_{\theta g}=-\frac{D_M}{r_s}\frac{\partial Y_g}{\partial \eta} \tag{28}$$

Dimensionless equations

The above equations and boundary conditions are dimensional zed using the following dimensionaless variables:

$$t^*=\frac{\upsilon_\infty Gr_T^{1/2}t}{4r_s^2};\quad u_r^*=u_r\frac{2r_s Gr_T^{-1/2}}{\upsilon_\infty};\quad u_\theta^*=u_\theta\frac{2r_s Gr_T^{-1/4}}{\upsilon_\infty},\mathrm{D}_M^*=\frac{D_M}{D_{M\infty}} \tag{29}$$

$$T^*=\frac{T-T_\infty}{T_S-T_\infty};\ Y^*=\frac{Y-Y_\infty}{Y_s-Y_\infty};\quad Q_R^*=\frac{Q_R}{Cp_\infty\left(T_f-T_\infty\right)},C_P^*=\frac{C_p}{C_{p\infty}} \tag{30}$$

$$\dot{m}^*=\frac{4\dot{\omega}_g r_s^2}{Gr_T^{0,5}\mu_\infty};\quad Gr_T=g\beta_T\frac{\left(2r_s\right)^3\left(T_\infty-T_f\right)}{\upsilon_\infty^2};\theta^*=\theta \tag{31}$$

$$Gr_M = g\beta_M \frac{(2r_s)^3 (Y_\infty - Y_s)}{\upsilon_\infty^2}; \quad (32)$$

r*=r/rs

$\mu^* = \frac{\mu}{\mu_\infty}$; $\rho^* = \frac{\rho}{\rho_\infty}$; $\vartheta^* = \frac{\vartheta}{\vartheta_\infty}$

The introduction of the above non-dimensional variables in the equations (18)-(24) leads to the following dimensionless equations:

Vapor phase

$$\frac{\rho_g^*}{r^{*2}}\frac{\partial}{\partial r^*}\left(r^{*2}u_{rg}^*\right) + \frac{\rho_g^* Gr_T^{-1/4}}{r^*\sin\theta^*}\frac{\partial}{\partial\theta^*}\left(u_{0g}^*\sin\theta^*\right) = 0 \quad (34)$$

$$\frac{\partial u_{rg}^*}{\partial t^*} + u_{rg}^*\frac{\partial u_{rg}^*}{\partial r^*} + \frac{u_{\theta g}^*}{r^* Gr_T^{1/4}}\frac{\partial u_{rg}^*}{\partial\theta^*} = \frac{\mu_g^*}{\rho_g^* r^{*2} Gr_T^{1/2}}\frac{\partial}{\partial r^*}\left(r^{*2}\frac{\partial u_{rg}^*}{\partial r^*}\right)$$

$$+\frac{\mu_g^*}{\rho_g^* Gr_T^{1/2}}\frac{1}{r^{*2}\sin\theta^*}\frac{\partial}{\partial\theta^*}\left(\sin\theta^*\frac{\partial u_{rg}^*}{\partial\theta^*}\right) + \left(T^* + \frac{Gr_M Y^*}{Gr_T}\right)\sin\theta^* \quad (35)$$

$$\frac{\partial T_g^*}{\partial t^*} + u_{rg}^*\frac{\partial T_g^*}{\partial r^*} + \frac{u_{\theta g}^*}{r^* Gr_T^{1/4}}\frac{\partial T_g^*}{\partial\theta^*} = \frac{\lambda_g^*}{\rho_g^* Cp_g^* r^{*2} Gr_T^{1/2}\mathrm{Pr}_\infty}\frac{\partial}{\partial r^*}\left(r^{*2}\frac{\partial T_g^*}{\partial r^*}\right)$$

$$+\frac{\lambda_g^*}{\rho_g^* Cp_g^* Gr_T^{1/2}\mathrm{Pr}_\infty}\frac{1}{r^{*2}\sin\theta^*}\frac{\partial}{\partial\theta^*}\left(\sin\theta^*\frac{\partial T_g^*}{\partial\theta^*}\right) + \frac{1}{\rho_g^* Cp_g^* Gr_T^{1/2}}\dot{m}_g^* Q_R^* \quad (36)$$

$$\frac{\partial Y_g^*}{\partial t^*} + u_{rg}^*\frac{\partial Y_g^*}{\partial r^*} + \frac{u_{\theta g}^*}{r^* Gr_T^{3/4}}\frac{\partial Y_g^*}{\partial\theta^*} = \frac{\rho_g^* D_M^*}{\rho_g^* r^{*2} Gr_T^{1/2}}\frac{1}{Sc_\infty}\frac{\partial}{\partial r^*}\left(r^{*2}\frac{\partial Y_g^*}{\partial r^*}\right)$$

$$+\frac{\rho_g^* D_M^*}{\rho_g^* Gr_T^{1/2}}\frac{1}{r^{*2}\sin\theta^*}\frac{\partial}{\partial\theta^*}\left(\sin\theta^*\frac{\partial Y_g^*}{\partial\theta^*}\right) + \frac{\dot{m}_g^*}{\rho_g^*(Y_S - Y_\infty)} \quad (37)$$

with

$$\dot{m}_g^* = \frac{4\omega_g \dot{r}_s^2}{Gr_T^{0,5}\mu_\infty} \quad (38)$$

liquid phase

$$\frac{\rho_l^*}{r^{*2}}\frac{\partial}{\partial r^*}(r^{*2}u_{rl}^*) + \frac{Gr_T^{-1/4}\rho_l^*}{r^*\sin\theta^*}\frac{\partial}{\partial\theta^*}(u_{0l}^*\sin\theta^*) = 0 \quad (39)$$

$$\frac{\partial u_{rl}^*}{\partial t^*} + u_{rl}^*\frac{\partial u_{rl}^*}{\partial r^*} + \frac{u_{\theta l}^*}{r^* Gr_T^{1/4}}\frac{\partial u_{rl}^*}{\partial\theta^*} = \frac{\mu_l^*}{\rho_l^* r^{*2} Gr_T^{1/2}}\frac{\partial}{\partial r^*}\left(r^{*2}\frac{\partial u_{rg}^*}{\partial r^*}\right)$$

$$+\frac{\mu_l^*}{\rho_l^* Gr_T^{1/2}}\frac{1}{r^{*2}\sin\theta^*}\frac{\partial}{\partial\theta^*}\left(\sin\theta^*\frac{\partial u_{rg}^*}{\partial\theta^*}\right) - g\beta_T T_l^*(T_s - T_\infty)\sin\theta^* \quad (40)$$

$$\frac{\partial T_l^*}{\partial t^*} + u_{rl}^*\frac{\partial T_l^*}{\partial r^*} + \frac{u_{\theta l}^*}{r^* Gr_T^{1/4}}\frac{\partial T_l^*}{\partial\theta^*} = \frac{\lambda_l^*}{\rho_l^* Cp_l^* r^{*2} Gr_T^{1/2}\mathrm{Pr}_\infty}\frac{\partial}{\partial r^*}\left(r^{*2}\frac{\partial T_l^*}{\partial r^*}\right)$$

$$+\frac{\lambda_l^*}{\rho_l^* Cp_l^* Gr_T^{1/2}\mathrm{Pr}_\infty}\frac{1}{r^{*2}\sin\theta^*}\frac{\partial}{\partial\theta^*}\left(\sin\theta^*\frac{\partial T_l^*}{\partial\theta^*}\right) + \frac{1}{\rho_l^* Cp_l^*}\dot{m}_l^* Q_R^* \quad (41)$$

The dimensionless initial and boundary conditions can be written as follows :

initial conditions

Liquid phase:

$$T_l^* = 1; \qquad u_{rl}^* = u_{rl0}^* = 0; u_{\theta l0}^* = 0 \quad (42)$$

-Gaseous phase:

$$Y_g^* = 1; \quad T_g^* = 1; \; u_{rg}^* = 0; \quad u_{\theta g}^* = 0 \quad (43)$$

- Dimensionless boundary conditions:

$$\frac{\partial T^*}{\partial r^*} = 0; \quad \frac{\partial u_{rl}^*}{\partial r^*} = 0; \quad \frac{\partial u_{\theta l}^*}{\partial r^*} = 0 \quad (44)$$

$$-\lambda_g^*\left.\frac{\partial T_g^*}{\partial r^*}\right|_g = \lambda_l^*\left.\frac{\partial T_l^*}{\partial r^*}\right|_l + \rho_g^* D_M^* Lv^*\left.\frac{\partial Y_g^*}{\partial r^*}\right|_g \quad (45)$$

$$\mu_g^* \frac{\partial u_{\theta g}^*}{\partial r^*}\Big|_g = \mu_l^* \frac{\partial u_{\theta l}^*}{\partial r^*}\Big|_l \quad (46)$$

$$u_{\theta g}^* = -D_M^* \frac{\partial Y_g^*}{\partial r^*}\Big|_g \quad (47)$$

-: $r \longrightarrow \infty$

$$T_g^* = 0;\ u_{rg}^* = u_{\theta g}^* = 0;\ Y_g^* = 0 \quad (48)$$

The surface mass fraction varies according to the saturated vapor pressure determined by Clausius Clapeyron equation, as reported by Abramzon & Sirignano and Dgheim *et al*. Therefore:

$$Y_s = Y_{S0} = \frac{P_{vs}}{\left(P_{vs} + \frac{(P_\infty - P_{vs})M_a}{M_f}\right)} \quad (49)$$

Where $P_\infty = 1atm$, $P_{vs}$is the saturated vapor pressure for hydrocarbon droplet and $T = (T_S - 273.15) * \frac{9}{5} + 32$
The latent heat is written as:

$$L = L_v \left(\frac{(T_{crit} - T_S)}{(T_{crit} - T_{ebn})}\right)^{0.38} \quad (50)$$

Where L_v represents the fuel latent heat of vaporization.

Table 1. Physical properties of heptane at lowand high temperatures

$\boldsymbol{273 < T < 380}$	$273 < \boldsymbol{T} < 1200$
$\boldsymbol{C_{pl}(\frac{J}{kg.K}) = 916.2 + 4.039 * T}$	$C_{pl} = T * \left(6.745 + T * (0.76 * 10^{-6} * T - 3.642 * 10^{-3})\right) - 51.33\left(\frac{J}{kg.K}\right)$
$\boldsymbol{\mu_l(kg/m.s) = 10^{(\frac{436.73}{T} - 4.878)}}$	$\mu_l(kg/m.s) = 0.8 * 10^{-6} + 1.8 * 10^{-6} * T$
$\boldsymbol{\rho_l(\frac{kg}{m^3}) = 1.212 * (\frac{T}{300})^{1.8}}$	$\rho_l(\frac{kg}{m^3}) = 0.1205 * P/T$
$\boldsymbol{L_v(\frac{J}{kg}) = 45\ 020}$	
$\boldsymbol{D_{air}(\frac{m^2}{s}) = 76.2 * 10^{-6} * T^{1.6/P}}$	

Numerical methodology

Numerical procedures

The Equations (35)-(41) associated to the boundary conditions (44)-(48)are solved using an implicit finite difference method and Thomas algorithm. A mesh sensitivity analysisleads to a time step of 0.015s for $\Delta\theta^* = 0.25$ and $\Delta\eta = 0.025$, that corresponding to a mesh of 40×72.

Procedure for transfers in the liquid and gaseous phases

The program was written in Fortran 90. The steps of this program are shown in the following flowchart:

- *initial data (velocity, temperature, pressure, radius, concentration, ...),*
- *geometrical quantities, values of the physical properties of the domain,*
- *initialization of the quantities in the liquid and gaseous phases,*
- *intermediate calculations,*
- *solving transfer equations in the vapor phase using Thomas' algorithm,*
- *solving transfer equations in the liquid phase using Thomas' algorithm,*
- *calculation of the temperature at the liquid-gaseous interface,*

- *check the continuity of the flux densities at the liquid-gaseous interface by testing the surface temperature: if the flux density test is less than 0.1, the calculation proceeds to the next step. Otherwise the calculation is repeated in step 4.*
- *test on the angle: if this angle is less than 90° the local Nusselt and Sherwood numbers are calculated; otherwise the calculation is stopped,*
- *test on the radius of the droplet: if the ratio between the calculated radius and the initial radius is less than 0.005 then the calculation is resumed in 4; otherwise the calculation is stopped.*

Model validation: In the case of evaporationin a quiescent gaseous media of an heptane droplet, it have been shown numerically and experimentally that squared radiusof the droplet gradually decreases until it evaporates completely(Dgheim *et al*. 2018). Ournumerical sofware has been validated by applying it to the problem of Bouaziz *et al*. 2002 and Dgheim *et al*. 2018that consists to the evaporation by natural convection of an heptane droplet. The initial radius of this heptane droplet equal to 7 mm and the duration of the evaporation of this droplet is equal to 2 mm. Figures 3, 4 and 5 represent respectively the temporal evolution ofthe radius squareand the one of the droplet surface temperature during the evaporation. As it can be seen in these figures,our results are in good agreement with those of Bouaziz *et al*. 2002 and Dgheim *et al*. 2018. The maximum deviation onradius and surface temperatureis about 2%.

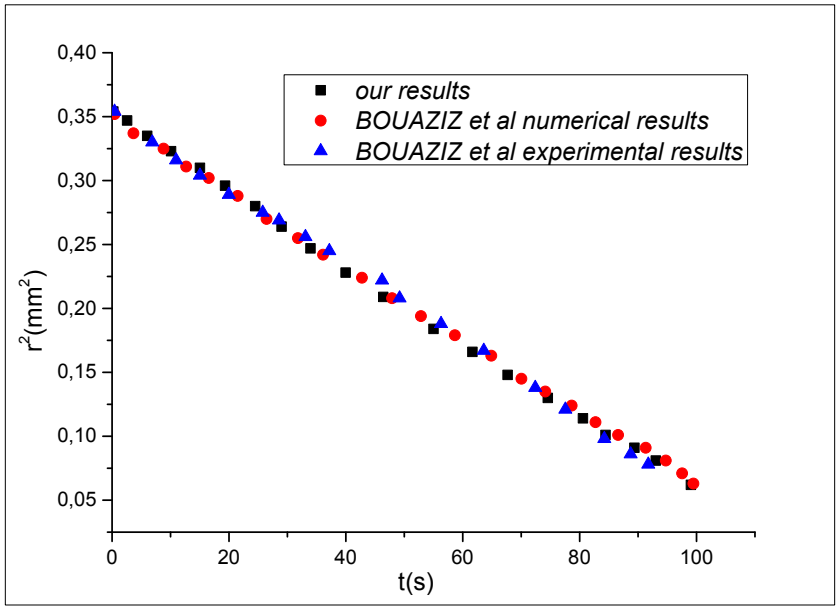

Figure 3: Comparison between our numerical results and the numerical and experimental results of (Bouaziz et al. 2002) for the regression of the radius square of the heptane droplet in evaporation in natural convection

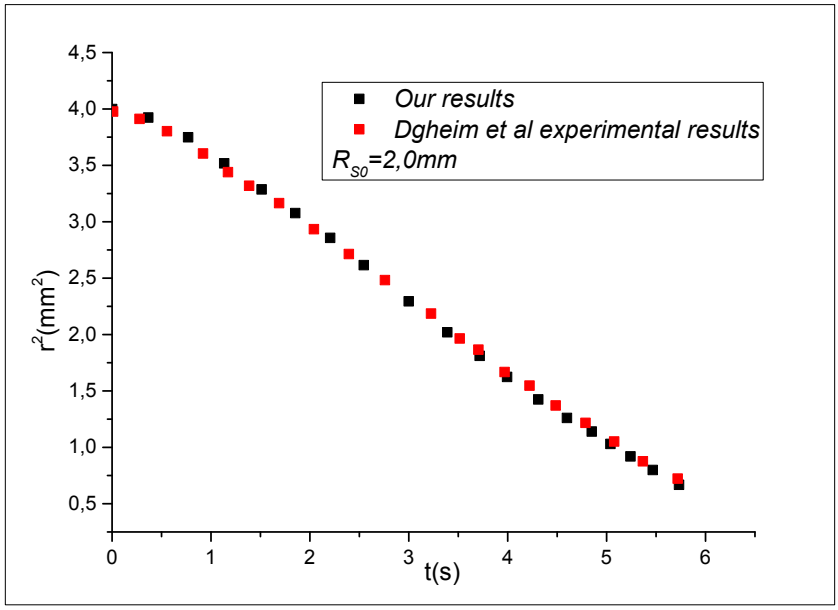

Figure 4. Comparison between our numerical results and the numerical and experimental results of Dgheim et al. 2018 for the regression of the radius square of the heptane droplet in evaporation in natural convection

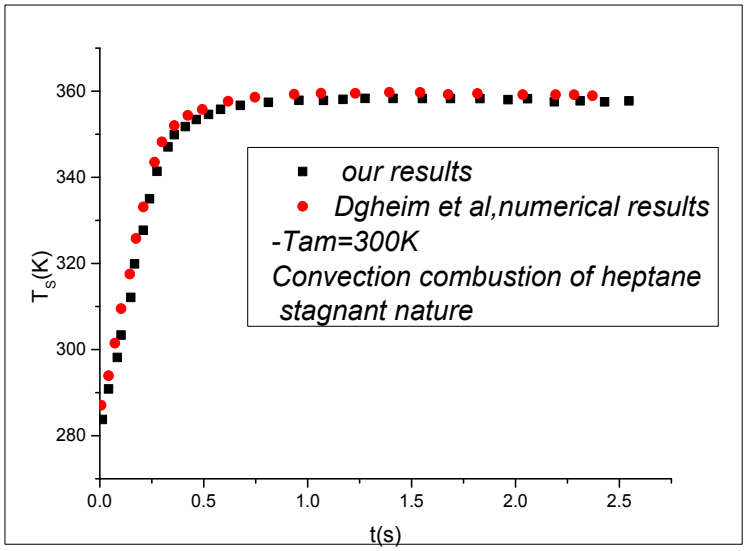

Figure 5. Comparison between our numerical results and the numerical and experimental results of Dgheim et al. 2018 for the surface temperature of the heptane droplet in evaporation in natural convection

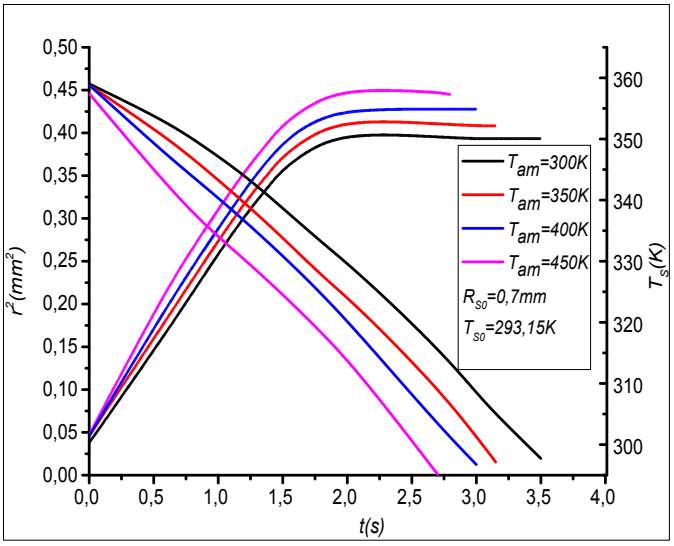

Figure 6. Square radius regressionand surface temperature evolution of heptane droplets in natural convection for different ambient temperatures

RESULTS AND DISCUSSION

As is can be seen in figures 6and 7 the duration of the complete evaporation of the heptane droplet is shorter as the gaseous medium temperature or the initial droplet radiusare high. The temperature of the droplet surface increases quickly over time until to reach at the end of the droplet evaporation the temperature of the gaseous medium. These results are corroborated by those on the time regression of the droplet square radius. Indeed, the amount of heat supplied by conduction-convection by the gaseous medium to the liquid droplet is higher as the difference between the initial temperature of the liquid droplet and the one of the gaseous medium is important. One part of this heat increases the temperature of the liquid phase and the remaining part allows evaporation of an amount of liquid that is more important as the amount of heat which is supplied to it by the gaseous medium is great. The figure 8 illustrates the effects of the heat and mass buoyancy forces on the duration of the complete evaporation of the liquid droplet. These buoyancy forces increases as the theta angle increases. Consequently, the heat and mass flux between the gaseous media and the liquid droplet are higher as the polar angle is great. It means that the evaporation is not homogeneous. So the shape of the liquid droplet supposed initially to be a sphere, is distorted over time ; *At the bottom of the liquid droplet, the radius square represents two slops where at theta equal 90° it decreases linearly.* As it can be seen in figures 9-12 whatever the values of the temperature of the gaseous media, of the initial droplet radius and of the polar angle, the effects of theses parameters on the liquid phase temperature of the heptane droplet are similar to those presented above on surface temperature of the droplet.

The liquid temperature increases as the distance from its center to its surface increases until its surface temperature at the liquid-vapor interface. The temperature continues its augmentation with the increase of the distance from the droplet center to reach high values in the vapor phase and finally returns back to the ambient temperature. In the whole cases, one can observe the evaporation of the liquid droplet explained by the regression of the liquid-vapor interface, and the evolution of the vapor phase (figure 9).

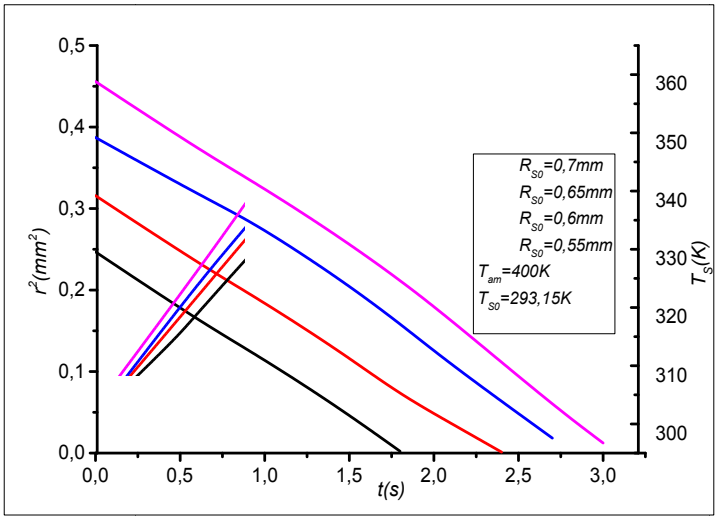

Figure 7. Square radius regressionand surface temperature evolution of heptane droplets in natural convection for different initial radii

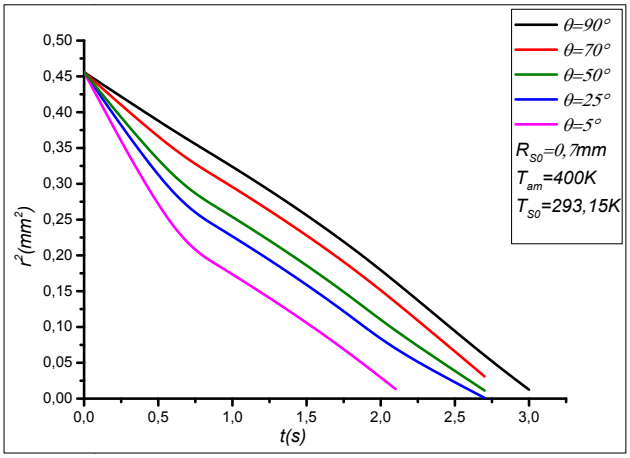

Figure 8. Square radius regression of heptane droplet in natural convection for different polar angles

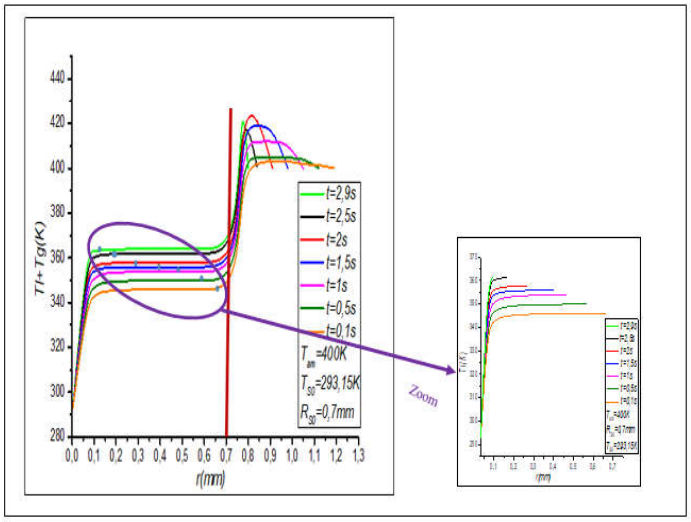

Figure 9. Radial evolution of liquid and vapor temperatures of the heptane droplet, in evaporation, in natural convection for different times

The progressive decrease of the initial radius of the liquid droplet due to its evaporation and the increase of the temperature of the surrounding environment (figures10, 12) have an important effect on the increase of the temperature gradient between the droplet surface and the ambient medium. This vapor gradient increases as the ambient temperature increases because the radial distance becomes smaller.

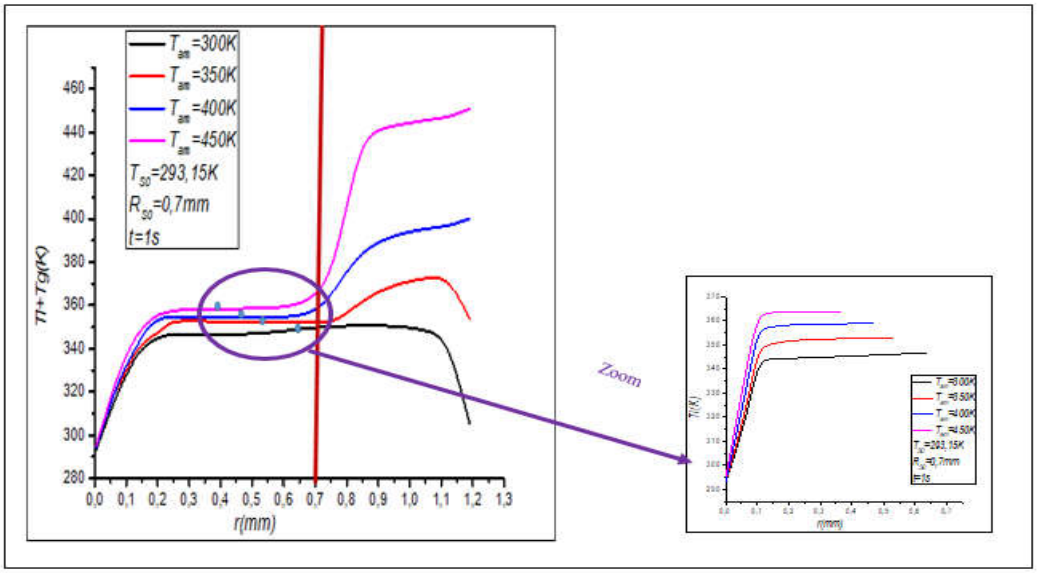

Figure 10: Radial evolution of liquid and vapor temperatures of heptane droplet, in evaporation, in natural convection, for various ambient temperatures

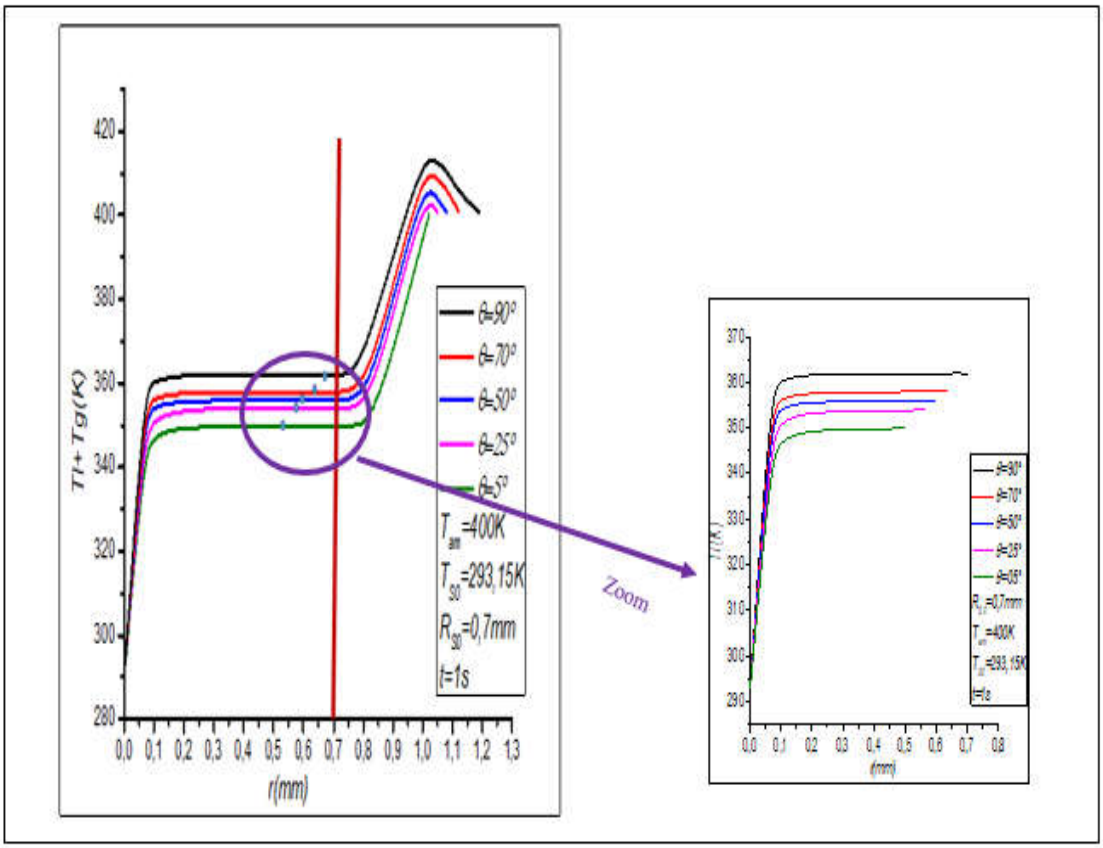

Figure 11: Radial evolution of liquid and vapor temperatures of heptanes droplet. in evaporation, in natural convection, for different polarangles

There is a gradual decrease of the vapor temperature to the ambient one away from the droplet surface. However, the increase of the ambient medium temperature causes rapid evaporation of the droplet due to the variation in air properties that is highly affected by the temperature (figure 10). On the other hand, when the droplet enters the hot environment and under the influence of the ambient temperature and the properties of the air, the droplet is exposed to the effects of shearing. Hot gases tend to penetrate the droplet by force. In fact, there is a transfer of heat from the environment to the interior of the liquid droplet through the surface of this last. The heat transfer promotes the evaporation of the liquid phase of the droplet. Therefore, the temperature increases from the surface of the droplet to the internal phase (the liquid phase). In addition, one noticed that at the bottom of the liquid

droplet (Θ=5°, Θ=25°),the evaporation process was much slower than that at the middle of the liquid droplet (Θ=70°, Θ=90°)(figure 11) because the buoyancy forces pushed the hot vapor from the bottom to the top of the liquid droplet. The effects of the values of the initial radius and the temperature of the gaseous media on the radial evolution of the heptane vapor mass fraction are similar to those on the vapor temperature (figures 13-16). The effects of the polar angle value considered on the vapor temperature and the heptane vapor mass fraction are also similar.

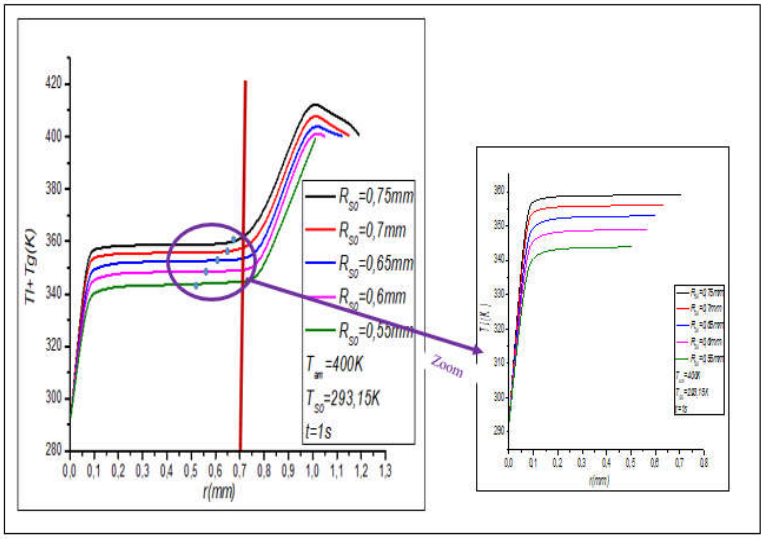

Figure 12: Radial evolution of liquid and vapor temperatures of heptane droplet, in evaporation, in natural convection, for different initial radii

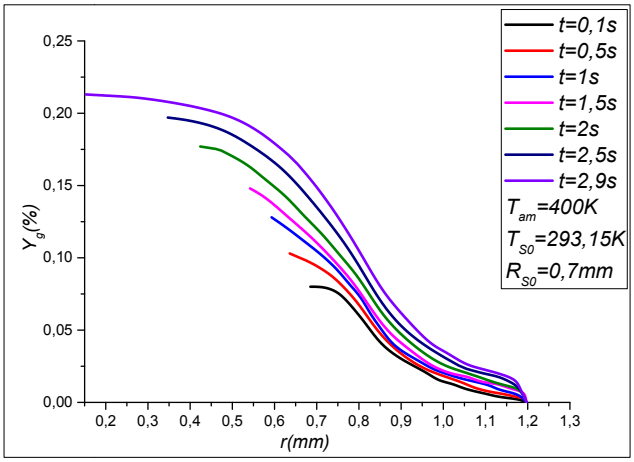

Figure 13: Radial evolution of the vapor mass fraction of heptane droplet in natural convection for different times

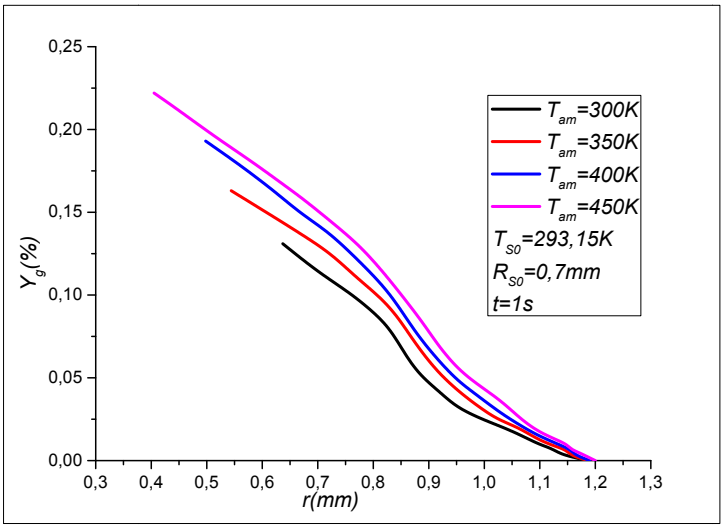

Figure 14: Radial evolution of the vapor mass fraction of heptane droplet in natural convection for various ambient temperatures

The heptane vapor mass fraction decreases from its value at the liquid-vapor interface corresponding to the vapor saturation mass fraction to the ambient one equal to zero far from the liquid droplet. The vapor saturation mass fraction is depending on the liquid phase temperature. Figure 15 shows the radial evolution of the heptane vapor mass fraction for different polar angles. These evolutions are similar to those on the vapor temperature presented above. Figure 16 shows for the evaporation duration considered that the heptane vapor mass fraction at the liquid -vapor interface is higher as the initial radius value of the heptane droplet is small. The greater the surface temperature is, the greater the mass fraction at the surface of the droplet. On the other hand, at the beginning of the evaporation process, the environment is dry and gradually becomes laden with vapor. For a specific mass fraction of vapor on the surface of the droplet, the vapor flow rate is highest when the mass fraction close to the droplet is low. This explains why the vapor flow rate is high at the beginning and then decreases afterwards. This decrease is, however, compensated at the leading edge by the increasing of the surface temperature and by the flow that discharges the vapor and maintains a high mass gradient.

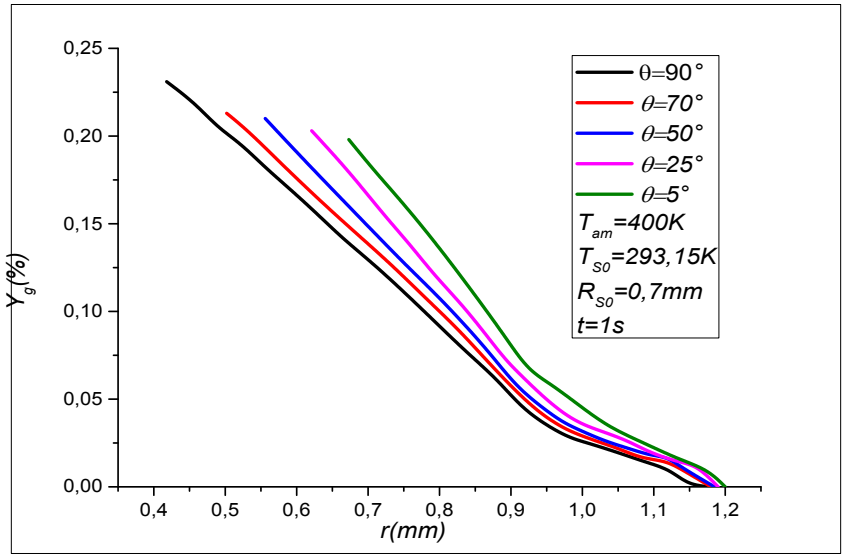

Figure 15: Radial evolution of the vapor mass fraction of heptanes Droplet in natural convection for different polarangles

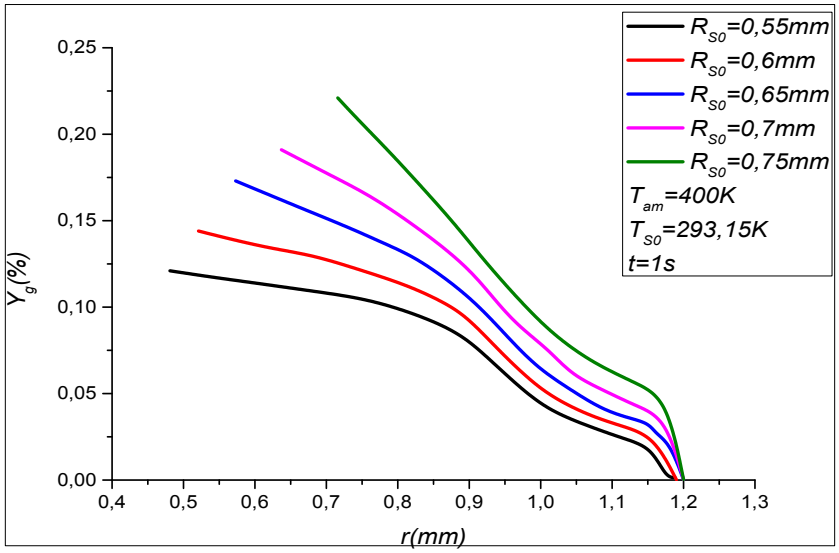

Figure 16: Radial evolution of the vapor mass fraction of heptane droplet in natural convectionfor different initial radii

The radial evolutions of the radial velocities in liquid and vapor phases of heptane dropletare presentedin figures 17-20. The radial velocity of the vapor phase increases from its value at the liquid-vapor interface to reach its maximum value before decreasing to the ambient medium value. One notesa similarity of the curves and a uniform overview of the evolution of the velocity distribution. In addition, it can be noted that the velocity of the gas phase of the droplet takes very low values over time as the droplet evaporates (figure 17). Indeed, theheat and mass transfers aredeveloped and propagated from the gaseous phase to the liquid one. In addition, evaporation phenomena linked to shear continuities of the velocities and to advection, and also to the quantity of movement, play an important part in the evolution of the velocities.

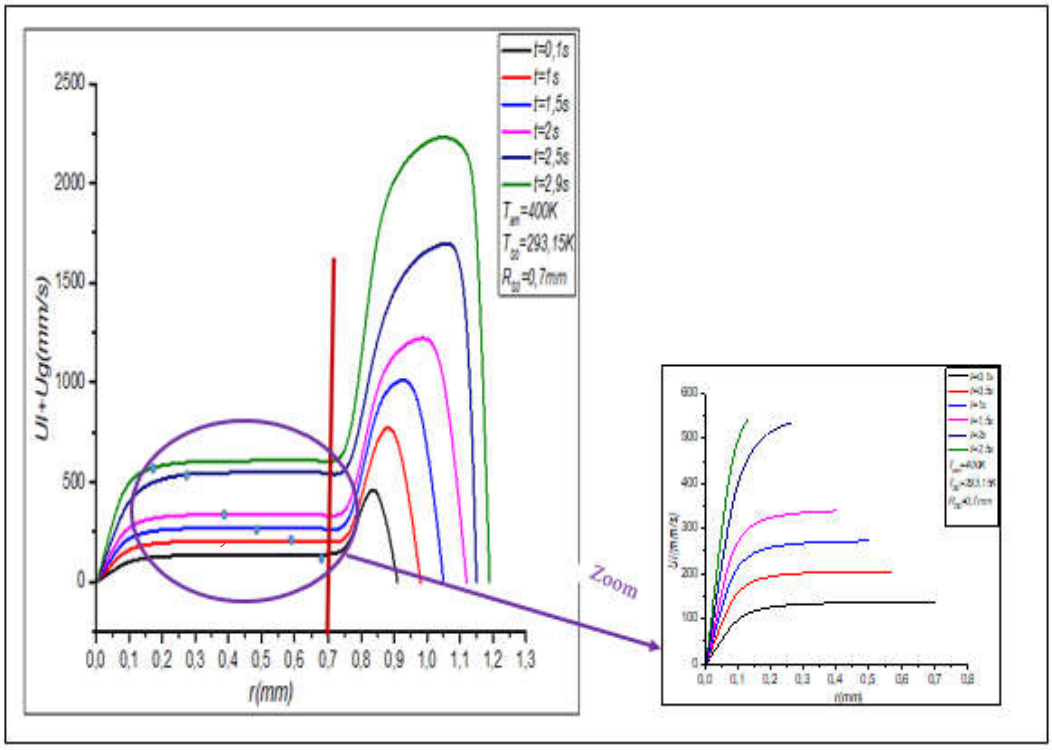

Figure 17: Radial evolution of the radial velocity of liquid and vapor phases of the heptane droplet, in evaporation, in natural convection for different times

A much finer analysis of the velocity results in the vapor phase shows that the flow distributed over the entire droplet distribution acts on the velocities, temperatures and mass fraction in both liquid and vapor phases.

The movement of the vapor is accompanied by the energy transport associated with the mass flows. As it can seen in figures 18 and 19, the effects of the gaseous medium temperature, and the initial radius of the heptane droplet on the radial evolution of the radial velocity in the liquid phase,are significantly only in the vicinity of the liquid-vapor interface.

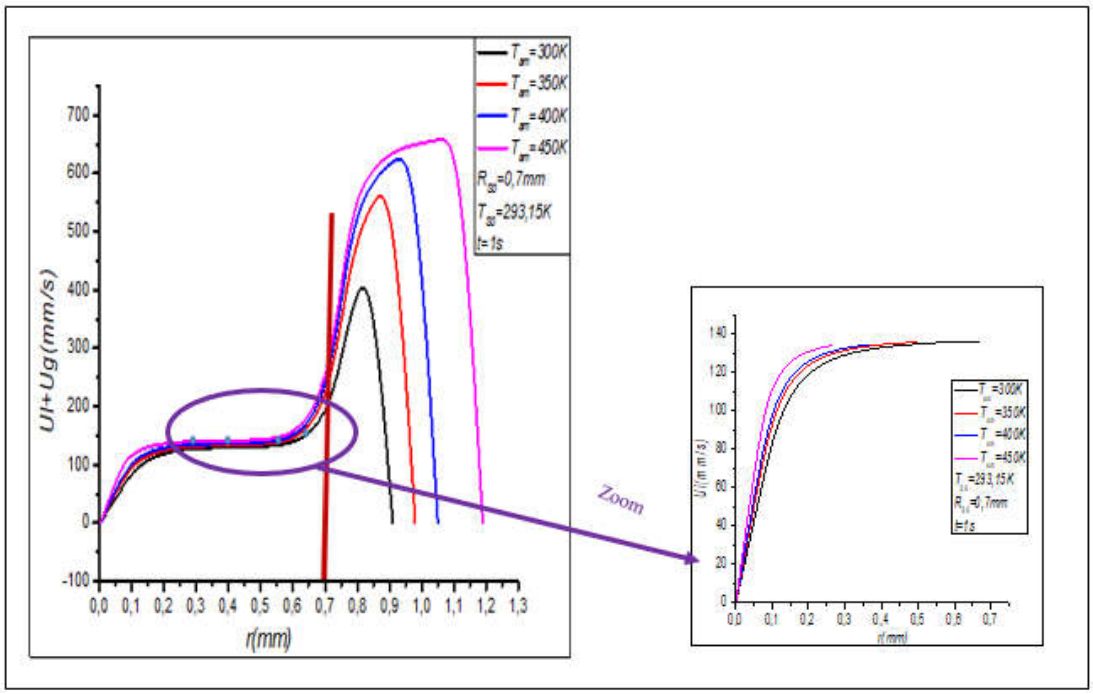

Figure 18: Radial evolution of the radial velocity of the liquid and vapor phases of the heptane droplet, in evaporation, in natural convection for different ambient temperatures

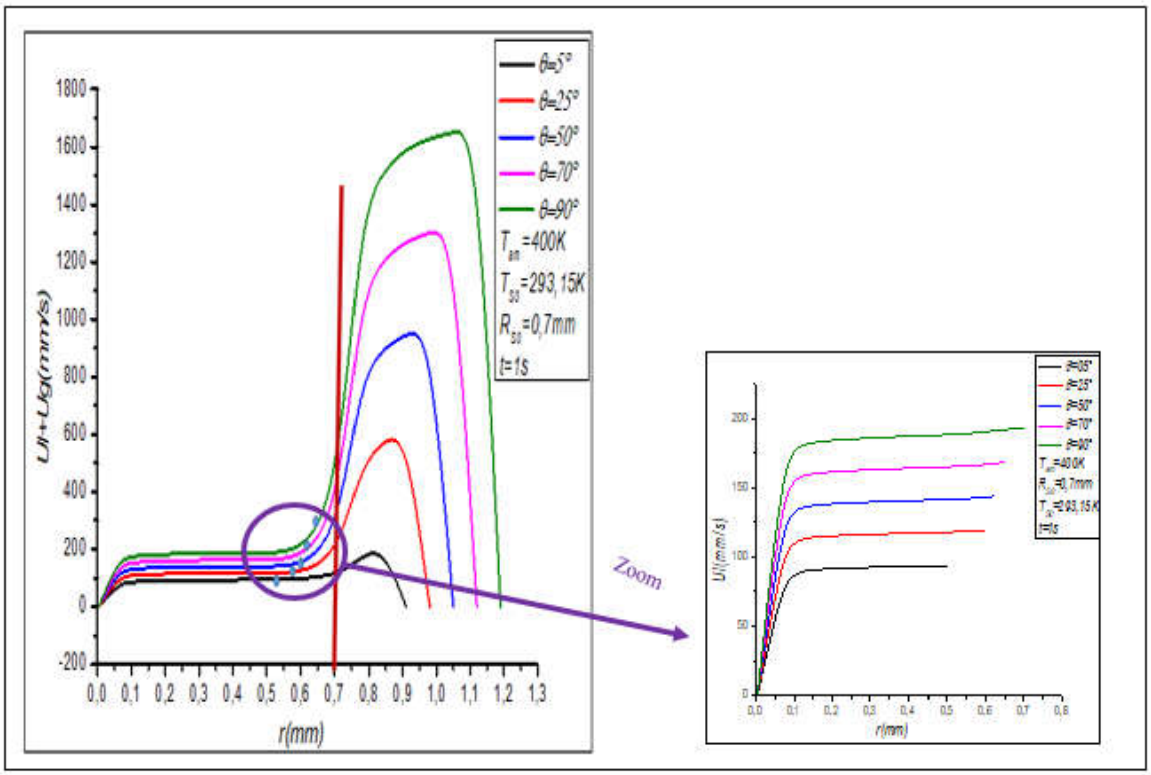

Figure 19: Radial evolution of the radial velocity of the liquid and vapor phases of the heptane droplet, in evaporation, in natural convection for different theta angles

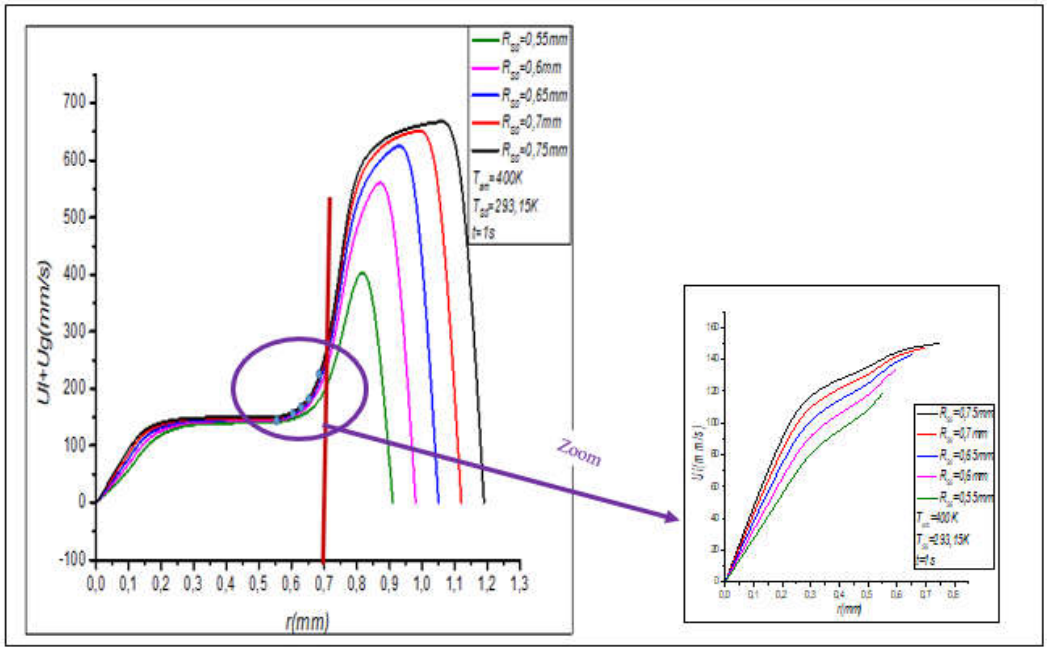

Figure 20. Radial evolution of the radial velocity of the liquid and vapor phases of the heptane droplet, in evaporation, in natural convection for different initial radii

This is due fromone hand, to the amount of the heat supplied to the liquid phase, which is for a given droplet size the more important as the temperature of the gaseous medium is high and from another hand, to an intensification of the transfer by natural convection in the liquid phase, all the more important as the quantity of liquid is high and therefore as the radius of the heptane droplet is large. Therefore, when the pure component evaporates in an ambient environment at high temperature (figure 18), a part of the heat perceived by the droplet from the ambient environment is used to heat the droplet and another one is used to evaporate it (this corresponds to the latent heat of the evaporation). The higher the temperature of the droplet increases, the more the heat perceived by the droplet decreases and the more energy the droplet consumes to evaporate, since it evaporates more**.** Figure 16 also shows that when theta angle increases the radial velocity value also increases. This is due to the heat and mass buoyancy forces along the liquid-vapor interface of the liquid droplet. The evolutions observed by the profiles of the droplet thickness for different temperatures of the ambient medium in which the droplet is placed, the theta angles and the initial radii of the droplet are shown in figures 21-23

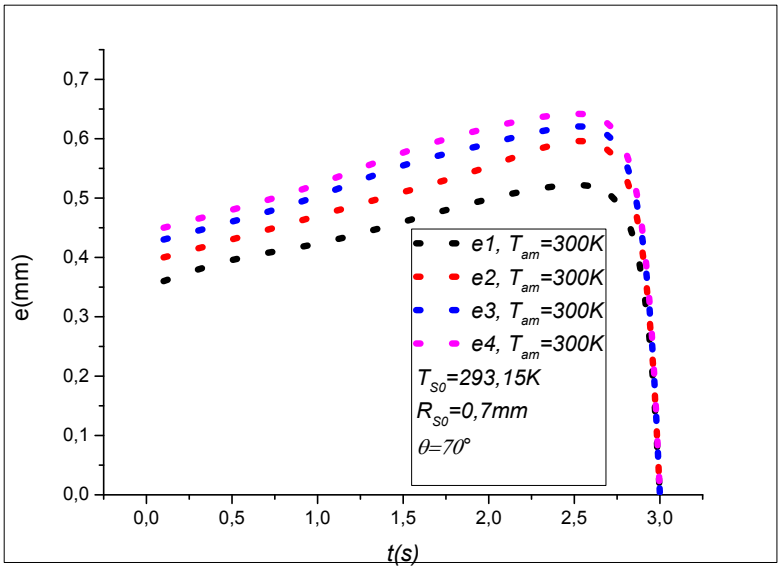

Figure 21: Evolution of the vapor thickness of the heptane droplet, in evaporation, in natural convection for different ambient temperatures

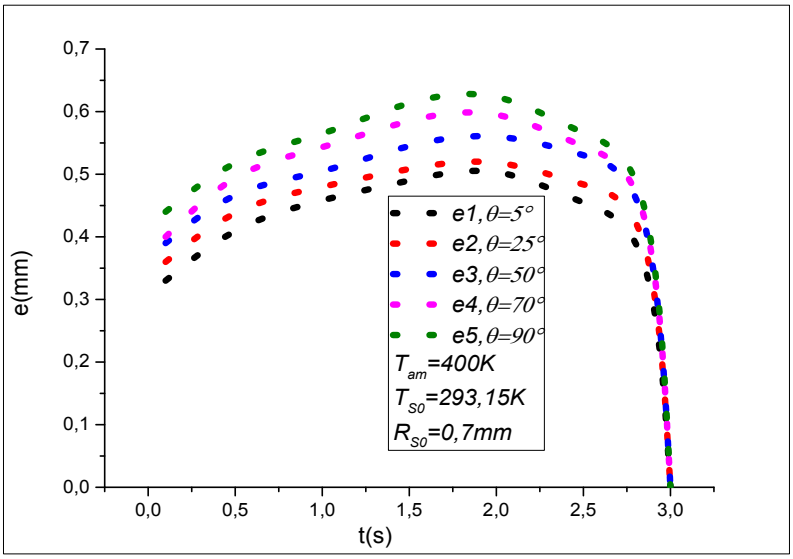

Figure 22: Evolution of the vapor thickness of the heptane droplet, in evaporation, in natural convection at different polar angles

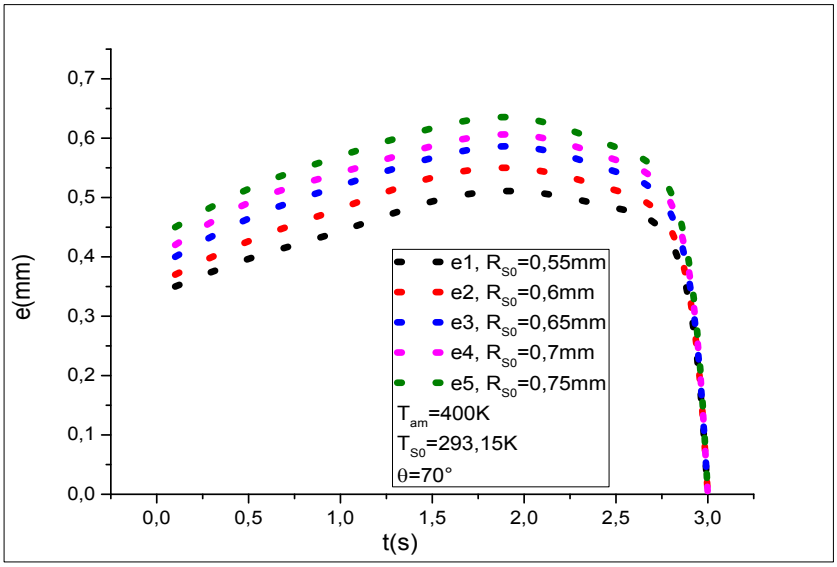

Figure 23: Evolution of the vapor thickness of the heptane droplet, in evaporation, in natural convection for different initial radii

These results suggest several observations:

- The calculated thicknesses are of the order of 32 to 65 mm
- Whatever the considered values of the temperature of the gaseous medium and the angle theta, the thickness of the vapor phase evolves, for a fixed droplet radius, over time as a parabola curve by reaching a zero value at the end of the evaporation process. It is higher as the initial radius of the droplet, the gaseous medium and the polar angle are large (figures 21-23). In addition, this thickness increases as the droplet initial radius is large. These results are corroborated by those presented previously on the heptane vapor temperature and mass fraction profiles.

Conclusion

This work focused on the evaporation of heptane droplet in natural convection. Naviers-Stockes equations coupled to heat and mass transfers equations in spherical coordinates are solved numerically using implicit finite difference method and Thomas' algorithm. Our numerical results are compared with those of Dgheim *et al* and Bouaziz *et al* and satisfactory qualitative and quantitative agreement is observed. The maximum relative error was of the order of 2%. Then, our computation is performed in order to study the effects of the variation of the different parameters such as the time, the ambient temperature, the theta angle and the initial radius of the heptane droplet on the evolution of the temperature and the velocity in the liquid and vapour phases, and the evolution of the mass fraction in the vapour phase. The evolution of the liquid-vapor interface (droplet radius) and the evolution of the vapor phase thickness are clearly observed for different physical parameters. At high ambient temperature, there is a decrease in temperature and velocity values in the liquid and vapour phases. The same phenomenon is observed for the mass fraction evolution in the vapor phase. Also, for large droplets (larger initial radius) and high theta angles, the temperature and velocity profiles have parabolic shape in the vapour phase. Thus, the vapor phase thickness is calculated and presented versus time for different physical parameters especially the theta angle. The none-sphericity of the evaporated heptane droplet is clearly observed.

Nomenclature

B	Spalding number	μ	dynamic viscosity, $kgm^{-1}s^{-1}$
Cp	specific heat, $Jkg^{-1}K^{-1}$	V	kinematic viscosity, m^2s^{-1}
L	latent heat, Jkg^{-1}	ρ	density, kgm^{-3}
P	pressure, atm	θ	polar angle, °
Pr	Prandtl number	Subscripts	
Sc	Schmidt number	a	air
T	temperature, K	f	fuel
t	time, s	l	liquid
u	velocity component in x direction, $m.s^{-1}$	m	mass
v	velocity component in y direction, $m.s^{-1}$	s	surface
Y	mass fraction	∞, amb	ambient medium
	Greek letters	$0, i$	initial
Δ	difference	Superscripts	
η	r/rs	*	dimensionless
λ	thermal conductivity, $Wm^{-1}K^{-1}$	-	mean

REFERENCES

Abramzon, B., et W. A. Sirignano. 1989. « Droplet Vaporization Model for Spray Combustion Calculations ». *International Journal of Heat and Mass Transfer* 32 (9): 1605–1618.

Ahmed, T., A. Kourmatzis, P.X. Pham, et A.R. Masria. 2018. « Droplet evaporation modeling of electrified fatty acid methyl esters ». *Fuel* 231: 244-52. https://doi.org/10.1016/j.fuel.2018.05.085.

Bouaziz, M., J. Dgheim, M. Grisenti, J. Bresson, et B. Zeghmati. 2002. « Experimental and Numerical Study in Evaporation of Hydrocarbon Droplet Surface Temperat ure » 53 (1).

Chahine, A.,J. Dgheim, 2017. « Contribution à l'étude numérique et expérimentale de l'évaporation et la combustion des gouttes d'hydrocarbures liquides en rotation. »

Chesneau, X. 1994. « Vaporisation et combustion de gouttes isolées de combustibles liquides. Influence de la pression ». Thèse de Doctorat, université d'Orléans.

Daho, T. 2008. « Contribution à l'étude des conditions optimales de combustion des huiles végétales dans les moteurs diesel et sur les brûleurs : cas de l'huile de coton ». BURKINA FAO: Université de Ouagadougou.

Dgheim, J., M. Abdallah, et N. Nasr. 2013. « Evaporation phenomenon past a rotating hydrocarbon droplet of ternary components ». *International Journal of Heat and Fluid Flow* 42 (avril): 224–235. https://doi.org/10.1016/j.ijheatfluidflow.2013.04.001.

gheim, J., M. Abdallah, et N. Nasr.. 2017. « Enhanced Evaporation of Droplet of Ternary Component Under the Effect of Thermo-physical and Transport Properties Variability », Arab J Sci Eng, , avril. https://doi.org/10.1007/s13369-017-2561-8.

Dgheim, J., A. Chahine, et J. Nahed. 2018. « Investigation on the droplet combustion in rotatory natural convection ». *Journal of King Saud University – Science*. https://doi.org/doi.org/10.1016/j.jksus.2018.02.007.

Frackowiak, B. 2007. « Approche expérimentale et simulation numérique des effets d'interactions entre gouttes en évaporation ». Toulouse: L'école nationale supérieure de l'aéronautique et de l'espace.

Godsave, G. A. E. 1953. « Studies of the combustion of drops in a fuel spray: The burning of single drops of fuel ». *in fourth international symposium on combustion*, 818-30.

Khiari, K. 2016. « Contribution à l'étude des propriétés thermo-physiques des biocarburants de seconde génération et leur influence sur le comportement des moteurs ». France: Ecole des Mines de Nantes.

Lupo, G., et C. Duwig. 2018. « A numerical study of ethanol–water droplet evaporation ». *Journal of Engineering for Gas Turbines and Power* 140 (2). https://doi.org/10.1115 / 1.4037753.

Mauduit, J. 1992. « contribution à l'étude de la vaporisation et de la combustion de gouttes isolées, introduction aux effets des hautes pressions ». France: ORLÉANS.

Merouane, H. 2013. « Étude de la vaporisation des gouttes de combustibles liquides en écoulement sous effet thermique ». Université des Sciences et de la Technologie d'Oran ″Mohamed Boudiaf ″.

Nath, Dipjyoti, Sukumar Pati, et Hema Sundar Raju. 2018. « Analysis of mixed convection past a heated sphere ». *Process Mechanical Engineering*, 1-16. https://doi.org/10.1177/0954408918780511.

NJE NJE, Christian. 2000. « Etude numérique de l'évaporation instationnaire d'un nuage de gouttes multicomposants ». France: Université de ROUEN.

Pan, Kuo-Long, et Ming-Chun Chiu. 2013. « Droplet combustion of blended fuels with alcohol and biodiesel/diesel in microgravity condition ». *Fuel* 113: 757–765. https://doi.org/10.1016/j.fuel.2013.03.029.

Pinheiro, A. P., J. M. Vedovoto, A. da Silveira Neto, et B. G. van Wachem. 2019. « Ethanol droplet evaporation: Effects of ambient temperature, pressure and fuel vapor concentration ». *International Journal of Heat and Mass Transfer* 143. https://doi.org/10.1016/j.ijheatmasstransfer.2019.118472.

Qubeissi, M. Al, S.S. Sazhin, C. Crua Turner, J., et M.R. Heikal. 2015. « Modelling of biodiesel fuel droplet heating and evaporation: Effects of fuel composition ». *Fuel* 154: 308–318. https://doi.org/10.1016/j.fuel.2015.03.051.

Sardar, R, S Majumder, A Sow, S Sen, A Mukhopadhyay, et A De. 2020. « Analysis of Multicomponent Gas Phase Diffusion Models in the Context of Droplet Evaporation ». *Proceedings of the 8th International and 47th National Conference on Fluid Mechanics and Fluid Power (FMFP)*.

Sazhin, S. S. 2018. « Modelling of Droplet Heating and Evaporation ». *Droplets and Spray*, 45-75.

Sazhin, Sergei S. 2017. « Modelling of fuel droplet heating and evaporation: Recent results and unsolved problems », Fuel, 196: 69–101. https://doi.org/10.1016/j.fuel.2017.01.048.

Tonini, S, et GE Cossali. 2012. « An analytical model of liquid drop evaporation in gaseous environment ». *Int J Ther Sci 57*, 45–53. https://doi.org/10.1016%2Fj.ijthermalsci.2012.01.017.

Zubkov, V. S, GE Cossali, S Tonini, O Rybdylova, C Crua, M Heikal, et S. S Sazhin. 2017. « Mathematical modelling of heating and evaporation of a spheroidal droplet ». *Int. J. Heat Mass Transfer* 108: 2181-90. https://doi.org/10.1016/j. ijheatmasstransfer.2016.12.074.

****